

Two-flux tunable Aharonov-Bohm caging in a photonic lattice

V. Brosco,¹ L. Pilozzi,^{1, a)} and C. Conti^{1, 2}

¹*Institute for Complex Systems, National Research Council, Via dei Taurini 19, 00185 Rome, Italy*

²*Department of Physics, University Sapienza, Piazzale Aldo Moro 5, 00185 Rome, Italy*

(Dated: 15 February 2021)

We study the Aharonov-Bohm caging effect in a one-dimensional lattice of theta-shaped units defining a chain of interconnected plaquettes, each one threaded by two synthetic flux lines. In the proposed system, light trapping results from the destructive interference of waves propagating along three arms, this implies that the caging effect is tunable and it can be controlled by changing the tunnel couplings J . These features reflect on the diffraction pattern allowing to establish a clear connection between the lattice topology and the resulting AB interference.

I. INTRODUCTION

In the early 1980s the geometrical interpretation of some phenomenological observables has introduced a new paradigm for the explanation of different effects¹, modifying, for example, our view of non-relativistic quantum phenomena such as the quantum Hall effect² and prompting new developments and discoveries of paramount relevance ranging from modern polarization theory³ to topological phases⁴.

Nowadays, the geometry of the Hilbert space, with its metric, defining the distance between two quantum states, and its connection⁵, fixing the phase accumulated along quantum trajectories, is a central object in condensed matter research, holding great promises for quantum information applications. In photonics and atomic physics the quest to engineer and control the geometric and topological properties of artificial lattices fostered remarkable efforts to implement effective electromagnetic fields for neutral particles.⁶ Just to mention a few examples, uniform magnetic fields were achieved in optical lattice-based experiments,⁷ in ring resonator arrays⁸, in optomechanical systems⁹. In photonic lattices, artificial gauge fields were generated using different techniques, *i.e.* introducing topological defects in two-dimensional structures,^{10,11} applying time-dependent modulation¹²⁻¹⁴, employing synthetic modal dimensions¹⁵ and, very recently, controlling the orbital angular momentum of the input light beam.¹⁶ What underlies most of the observations carried out in the above systems is the first discovered and most basic consequence of the existence of gauge-fields, the Aharonov-Bohm (AB) effect¹⁷. The paramount importance of this effect ranges from metrological applications to basic physics¹⁸. It is a non-local effect, arising from the interference of electron beams traveling along paths enclosing a magnetic flux. As first recognized by Wu and Yang¹⁹, it naturally leads to the concept of path-dependent phase factor as a basis to describe electromagnetism and gauge theories in general. Furthermore, as it clearly emerges in path-integral derivations, AB interference reflects the multiply connected nature of the space and it may have impressive consequences on transport. An example is Aharonov-Bohm caging a single-particle localization effect arising from the interplay between the lattice struc-

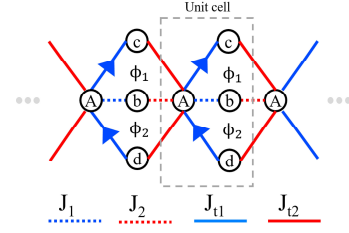


FIG. 1. Sketch of the structure of the θ -lattice composed of interconnected plaquettes, each one threaded by two synthetic flux lines, ϕ_1 and ϕ_2 . An arrow means a phase $e^{i\phi}$.

ture and the magnetic flux, first predicted by J. Vidal et al.²⁰ for two-dimensional electronic lattices and subsequently extended and experimentally verified in different contexts,²¹⁻²³ including photonic lattices, see *e.g.* Refs. 12, 24, and 25.

In the present work we study the propagation of light through a one-dimensional array of theta-shaped plaquettes threaded by two fluxes as shown in Fig. 1, that, for brevity, we call θ -lattice. The presence of two fluxes allows us to investigate in a simple but non-trivial framework the signatures of Aharonov-Bohm interference on diffraction patterns highlighting its topological significance and showing how in this case the caging effect becomes fully tunable.

II. MODEL

We consider a one-dimensional lattice of theta-shaped units as shown in Fig.1. Its unit cell consists of four sites indicated respectively as A , b , c and d . The three arms of each ring, defined by the sites A_n , A_{n+1} and respectively b_n , c_n and d_n , enclose two synthetic flux lines, indicated respectively as ϕ_1 and ϕ_2 .

The Hamiltonian of the θ -lattice can thus be written as:

$$H = \sum_n [J_{t1} (a_n^\dagger c_n e^{-i\phi_1} + a_n^\dagger d_n e^{i\phi_2}) + J_{t2} (a_n^\dagger d_{n-1} + a_n^\dagger c_{n-1}) + J_1 a_n^\dagger b_n + J_2 a_n^\dagger b_{n-1} + \text{H.c.}] \quad (1)$$

where m_n , m_n^\dagger with $m = a, b, c, d$ are bosonic annihilation and creation operators corresponding to the sites A, b, c, d of the

^{a)}Electronic mail: laura.pillozzi@isc.cnr.it

cell n . Switching to k -space we obtain:

$$\mathcal{H}(k, \phi_1, \phi_2) = \sum_k [J_b(k) a_k^\dagger b_k + J_c(k, \phi_1) a_k^\dagger c_k + J_d(k, \phi_2) a_k^\dagger d_k + \text{H.c.}] \quad (2)$$

where $m_k = \frac{1}{\sqrt{N}} \sum_n m_n e^{ikn}$, with N denoting the number of unit cells in the lattice, while $J_b(k) = J_1 + J_2 e^{-ik}$ and $J_c(k, \phi) = J_d(k, -\phi) = J_{t1} e^{-i\phi} + J_{t2} e^{-ik}$, where J_1 and J_{t1} and J_2 and J_{t2} denote the intra- and inter-cell hopping amplitudes. The ϕ_1, ϕ_2 dependence of J_c and J_d is due to the presence of the synthetic gauge fields. We note that setting $J_{t2} = J_{t1} = 0$ the θ -lattice reduces to the non-abelian Lieb lattice model²⁶ while setting $J_b = 0$ it reduces to the standard rhombi chain with a flux $\phi_T = \phi_1 + \phi_2$.

The Hamiltonian $\mathcal{H}(k, \phi_1, \phi_2)$ is invariant, up to a gauge transformation, under permutations of the three arms b, c, and d, *i.e.* under elements of the non-Abelian group S_3 . This implies that the state

$$|\phi_s(k)\rangle = J_b|b_k\rangle + J_c|c_k\rangle + J_d|d_k\rangle, \quad (3)$$

invariant under elements of S_3 , yields two dispersive modes:

$$|\psi_{\pm}(k)\rangle = \frac{1}{\sqrt{2}} \left[|a_k\rangle \pm \frac{|\phi_s(k)\rangle}{\Delta(k, \phi_1, \phi_2)} \right] \quad (4)$$

with longitudinal momenta $\kappa_{\pm}(k, \phi_1, \phi_2) = \pm \Delta(k, \phi_1, \phi_2)$ and

$$\Delta(k, \phi_1, \phi_2) = \sqrt{|J_b(k)|^2 + |J_c(k, \phi_1)|^2 + |J_d(k, \phi_2)|^2}. \quad (5)$$

On the other hand, the states

$$|w_1\rangle = J_b^*|c_k\rangle - J_c^*|b_k\rangle \quad (6)$$

$$|w_2\rangle = J_b^*|d_k\rangle - J_d^*|b_k\rangle \quad (7)$$

spanning a two-dimensional non-invariant subspace of S_3 must be degenerate for all J 's. These states thus yields two non-dispersive modes for any ϕ_1 and ϕ_2 with longitudinal momentum $\kappa = 0$. The presence of these modes underlies an $SU(2)$ non-abelian gauge symmetry.

The overall structure of the spectrum for $\phi_1 = \phi_2 = \phi$ with $J_i = J$ for $i = (1, 2, t1, t2)$ can be seen in Fig.2a) showing a band crossing at $(k, \phi) = (\pi, 0)$ and gaps for $\phi \neq 0$. We notice that for certain values of the coupling J and flux per plaquette *all* bands in the energy dispersion became flat as indicated by the red dashed lines. This condition, a result of a destructive interference induced by the synthetic magnetic field, gives rise to light trapping and corresponds to the AB caging effect.

III. AHARONOV-BOHM CAGING

A peculiarity of the two-flux model is that the caging arises due to the destructive interference of waves propagating along three arms. This implies that, at variance with the standard two-arm single-flux AB cages²⁷, the values of ϕ_1 and ϕ_2 where the caging effect appears can be controlled by changing the tunnel couplings J . We remark that when caging arises due to

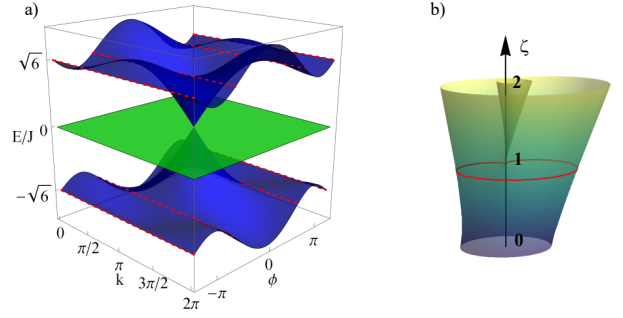


FIG. 2. a) Spectrum of $\mathcal{H}(k, \phi_1, \phi_2)$ for $J_i = J$ with $i \in (1, 2, t1, t2)$ and $\phi_1 = \phi_2 = \phi$. The red dashed lines show the ϕ values that give four flat bands. b) Cylindrical plot of the surface $\rho(\phi, \zeta) = 1 + \zeta \cos(\phi)$

the destructive interference of waves propagating along two arms it has to be necessarily located at $\phi = \pi$, *i.e.* the total amplitude is given by the sum of two identical terms having opposite sign. On the contrary, as stated above, in the θ -lattice we find different caging conditions depending on the tunnel couplings. In particular, when all J 's are equal, caging appears for $\phi_1 = \phi_2 = 2\pi/3$ and $\phi_1 = \phi_2 = 4\pi/3$ reflecting the trigonal symmetry of the unit cell. For arbitrary values of the J 's and $\phi_1 = \phi_2 = \phi$ the condition to have dispersionless bands can be written as follows

$$1 + \zeta \cos(\phi) = 0 \quad (8)$$

where $\zeta = 2J_{t2}J_{t1}/(J_1J_2)$. In Fig.2b) we show a cylindrical plot of the surface $\rho(\phi, \zeta) = 1 + \zeta \cos(\phi)$, where we clearly distinguish three cases: for $\zeta > 1$ we have two values of $\phi \in [0, 2\pi]$ where Eq.(8) is satisfied, for $\zeta < 1$ the caging condition is never fulfilled, while for $\zeta = 1$ Eq.(8) admits only the solution $\phi = \pi$ as in the case of the standard two-arm AB caging.

To further analyze how caging arises when $\phi_1 = \phi_2 = \phi$, in Fig.3 (a-e) we show the evolution of the quasi-energy spectrum support as ζ increases from $\zeta = 0$ to $\zeta = 2$. At $\zeta = 0$, corresponding to $J_{t1}J_{t2} = 0$, the spectrum is clearly ϕ -independent; as we increase ζ we find a pseudo-localization region around $\phi = \pi$ that evolves in a fully localized spectrum for $\zeta = 1$; eventually for $\zeta > 1$, the spectrum support shows two nodes, signaling the emergence of genus 2 AB caging.

Let us now consider the light dynamics in the different caging regimes. As discussed by several Authors, see *e.g.*^{27,28}, assuming evanescent coupling of single-mode waveguides, it is described by the following coupled mode equations:

$$\begin{cases} i\partial_z a_n = J_1 b_n + J_2 b_{n-1} + J_{t1}(e^{i\phi_1} c_n + e^{-i\phi_2} d_n) + J_{t2}(c_{n-1} + d_{n-1}) \\ i\partial_z b_n = J_1 a_n + J_2 a_{n+1} \\ i\partial_z c_n = J_{t1} e^{-i\phi_1} a_n + J_{t2} a_{n+1} \\ i\partial_z d_n = J_{t1} e^{i\phi_2} a_n + J_{t2} a_{n+1} \end{cases} \quad (9)$$

where ∂_z indicate the partial derivative with respect to z . Solving numerically the above equations on a finite lattice with N

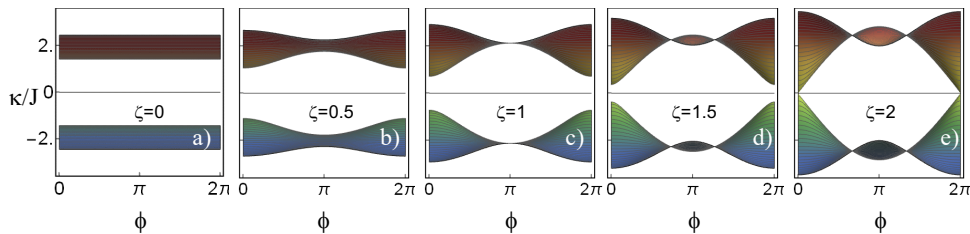


FIG. 3. Spectrum support on the (κ, ϕ) plane for different values of ζ .

unit cells ($4N$ sites) and open boundary conditions yields the results shown in Figs. 4 and 5.

In Figure 4 we simulate the propagation of a light beam injected at $z = 0$ in a θ -lattice consisting of N unit cells, $4N$ waveguides, with homogeneous tunnel couplings $J_i = J$ and fluxes $\phi_1 = \phi_2 = \phi = 2\pi/3$. For these parameters the dispersive bands κ_{\pm} become flat and, independently of the precise position and energy of the incoming beam, light gets trapped on a cluster of few waveguides. Only the structure of the caging cluster depends on the initial condition. This is due to the fact that, depending on the initial condition, different localized bands enter the dynamics. When the light is injected in a site A only the upper and lower bands are dynamically occupied; caging then implies that only the waveguide A_n and the six surrounding waveguides b_n, c_n, d_n and $b_{n-1}, c_{n-1}, d_{n-1}$ are populated as shown in Fig.4a). The wavelength, λ_0 , of the oscillations between the upper and lower bands is clearly given by the inverse of the spectral gap *i.e.* $\lambda_0 = 1/(2\Delta_0)$ with $\Delta_0 = \Delta(k, 2\pi/3, 2\pi/3) = \sqrt{6}J$. A somewhat similar situation arises when light is injected symmetrically in the waveguides b_n, c_n, d_n , *i.e.* creating the initial state $|\psi_0\rangle = \frac{1}{\sqrt{3}}(|b_{n_0}\rangle + |c_{n_0}\rangle + |d_{n_0}\rangle)$. The peculiar structure of the initial state implies that in this case, shown in Fig. 4(b), the light beam undergoes oscillations between the cell n and $n+1$ along z without modifying its shape. Eventually in Fig. 4(c) we show the propagation of a light beam injected from the site c_n . In this case the evolution involves also the degenerate bands and the signal spreads over three unit cells.

When the caging condition is not fulfilled, light spreads to the entire lattice. This situation is considered in Fig.5 where we set $\phi_1 = \phi_2 = \pi$ and the other parameters as in Fig. 4. These values of the fluxes are special under many respects:

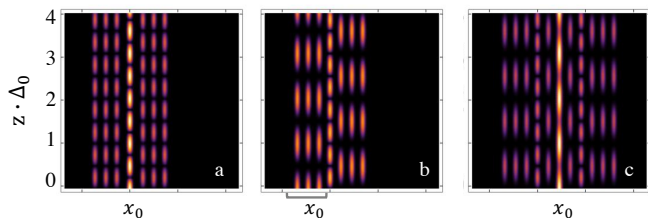


FIG. 4. Light dynamics in the presence of AB caging for three different injection configurations: (a) $|\psi_0\rangle = |a_{n_0}\rangle$, (b) $|\psi_0\rangle = \frac{1}{\sqrt{3}}(|b_{n_0}\rangle + |c_{n_0}\rangle + |d_{n_0}\rangle)$ and (c) $|\psi_0\rangle = |c_{n_0}\rangle$. Lattice parameters: $J_1 = J_2 = J_{t1} = J_{t2} = J$, $\phi_1 = \phi_2 = \phi = 2\pi/3$, $\Delta_0 = \sqrt{6}J$, $N = 40$, $n_0 = 20$.

first, as discussed in the following section, they yield, Fig.5a), a weaker dispersion as compared *e.g.* to the case $\phi_1 = \phi_2 = 0$, and second, they yield destructive Aharonov-Bohm interference on specific sites of the array. For example, as shown in Fig.5(b), for a "b" type injection waveguide, the propagation does not involve the sites "c" and "d" in the same plaquette, while, as shown in Fig.5(c), for a "c" type injection waveguide, the propagation does not involve the site "b" in the same plaquette. This is due to the fact that, at $\phi_1 = \phi_2 = \pi$ there are two tunneling paths from b to c and from b to d having opposite signs and equal amplitudes.

IV. SIGNATURES OF AHARONOV-BOHM INTERFERENCE IN THE DIFFRACTION PATTERNS

Beside inducing AB caging, synthetic gauge fields modulate light propagation in photonic lattices through AB interference, mimicking the action of their electromagnetic counterparts and yielding synthetic-flux dependent diffraction effects. Purpose of the present section is to highlight how these effects arise in the θ -lattice. To characterize diffraction for different values of the synthetic fluxes we will focus on two quantities, namely, the inverse participation number, P^{-1} , defined as

$$P^{-1} = \sum_x |\Psi_x|^4, \quad (10)$$

where Ψ_x denotes the field's amplitude at position $x = na$ along the lattice, with "a" the lattice period, and the average square width, W^2 , defined as

$$W^2 = \frac{\langle x^2 \rangle - \langle x \rangle^2}{N^2} \quad (11)$$

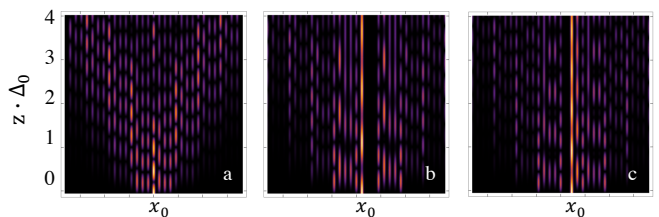


FIG. 5. Dispersive light dynamics for $\phi_1 = \phi_2 = \phi = \pi$, *i.e.* away from the AB caging condition, for three different injection configurations: (a) $|\psi_0\rangle = |a_{n_0}\rangle$, (b) $|\psi_0\rangle = |b_{n_0}\rangle$ and (c) $|\psi_0\rangle = |c_{n_0}\rangle$. Other lattice parameters as in Fig. 4.

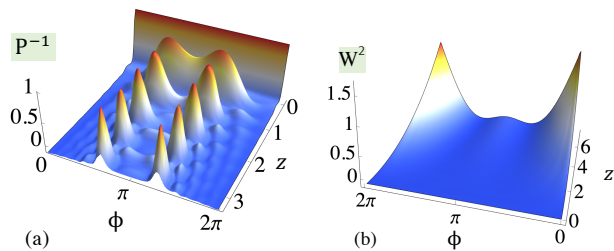


FIG. 6. Inverse participation ratio (a) and average width (b) as functions of z and ϕ . Other lattice parameters as in Fig. 4

with $\langle x^\alpha \rangle = \sum_x x^\alpha |\psi_x|^2$. The inverse participation number is always smaller or equal 1 and it gives a measure of the number of sites where photons are confined, specifically we have $P = 1$ when light is confined to a single waveguide and $P \sim m$ when light is confined to a cluster of m waveguides. The average width W is useful to characterize how the signal disperse, it equals zero in the presence of caging and in standard photonic waveguide lattices it grows as z^2 . In Figure 6(a) we plot the participation ratio as a function of z and ϕ for a lattice with homogeneous tunnel couplings and fluxes, *i.e.* $\phi_i = \phi$ and $J_i = J_{ii} = J$ with $i = 1, 2$. We assume that the system is initially prepared in the fully localized state $|a_{n_0}\rangle$, at $z = 0$ we thus have $P^{-1} = 1$ independently of ϕ . As z increases, light start dispersing and we clearly see the emergence of two peaks at $\phi = 2\pi/3$ and $\phi = 4\pi/3$ due to AB caging. We also notice that P^{-1} has a strongly oscillating behavior with z that is associated with dynamic oscillations between different bands. The presence of these oscillations may hinder the characterization of the difference interference regimes by simply measuring the amplitude of the fields in a small cluster of sites for a given propagation length $z = \bar{z}$. For this purpose, the square width W^2 defined in Eq.(11) may be more appropriate as we show in Figure 6(b). There, we notice in particular the emergence of a smooth double-well structure associated with AB interference. Having a monotonic behavior as a function of z , W can be used to characterize the different diffraction regimes for different values of the synthetic fluxes and J 's. This is what we do in Fig. 7 (a-b) to illustrate the tunability of the caging effect in the θ -lattice. In Fig. 7 (a) we show a density plot of the width W calculated at $zJ = 10$ for the system initially prepared in the state $|a_{n_0}\rangle$, as a function of ϕ_1 and ϕ_2 for homogeneous tunnelings. We clearly see that the contour $W = 0.5$ represented by the dashed black line essentially allows us to distinguish between a weakly dispersing region including the caging points $\phi_1 = \phi_2 = 2\pi/3$ and $\phi_1 = \phi_2 = 4\pi/3$ and a strongly dispersing region for $\phi \lesssim \pi/2$. In Fig. 7 (b) we plot $W_{z=10J}$ as a function of ϕ and J_{12} setting all other tunnel couplings to J . In this figure the black dashed line indicates the caging condition given by Eq. (8). We notice that when J_{12} becomes much larger than J the tunability essentially disappears, this is due to the fact that increasing J_{12} corresponds to decrease the weight of interference paths going through the site b bringing the lattice back to the single flux regime.

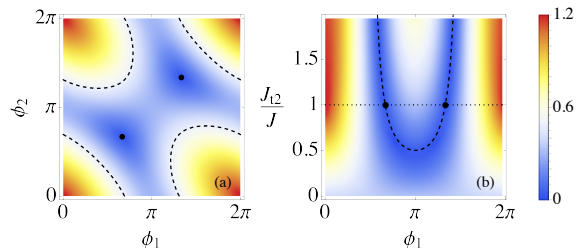


FIG. 7. Density plot of the width W as a function of ϕ_1 and ϕ_2 and as a function of J_{12} and $\phi = \phi_1 = \phi_2$.

V. CONCLUSIONS

We presented a theoretical study of transport of light in a strip of theta-shaped plaquettes subjected to synthetic magnetic fields. We showed how to realize Aharonov-Bohm cages that prevent the photon beam to escape from finite clusters. Suitably chosen fluxes with selected input configurations enables tuning the cage size. Our results have relevance for fundamental properties of topological lattice and various applications as in non-diffractive image transmission schemes^{29,30}, all-optical logic gates³¹ and optical data processing.

DATA AVAILABILITY

The data that support the findings of this study are available from the corresponding author upon reasonable request.

ACKNOWLEDGMENTS

Useful discussions with R. Fazio are gratefully acknowledged.

We acknowledge funding from QuantERA ERA-NET Co-fund (Grant No. 731473, project QUOMPLEX) and H2020 PhoQus project (Grant No. 820392).

- ¹D. Vanderbilt, *Berry Phases in Electronic Structure Theory* (Cambridge University Press, 2018).
- ²D. J. Thouless, M. Kohmoto, M. P. Nightingale, and M. den Nijs, “Quantized hall conductance in a two-dimensional periodic potential,” *Physical Review Letters* **49**, 405–408 (1982).
- ³R. Resta, “Macroscopic electric polarization as a geometric quantum phase,” *Europhysics Letters (EPL)* **22**, 133–138 (1993).
- ⁴M. Z. Hasan and C. L. Kane, “Colloquium: Topological insulators,” *Rev. Mod. Phys.* **82**, 3045–3067 (2010).
- ⁵F. Wilczek and A. Shapere, *Geometric Phases in Physics* (WORLD SCIENTIFIC, 1989).
- ⁶M. Aidelsburger, S. Nascimbene, and N. Goldman, “Artificial gauge fields in materials and engineered systems,” *Comptes Rendus Physique* **19**, 394–432 (2018).
- ⁷M. Aidelsburger, M. Atala, S. Nascimbene, S. Trotzky, Y.-A. Chen, and I. Bloch, “Experimental realization of strong effective magnetic fields in an optical lattice,” *Physical Review Letters* **107**, 255301 (2011).
- ⁸M. Hafezi, S. Mittal, J. Fan, A. Migdall, and J. M. Taylor, “Imaging topological edge states in silicon photonics,” *Nature Photonics* **7**, 1001–1005 (2013).

- ⁹M. Schmidt, S. Kessler, V. Peano, O. Painter, and F. Marquardt, “Optomechanical creation of magnetic fields for photons on a lattice,” *Optica* **2**, 635 (2015).
- ¹⁰M. C. Rechtsman, J. M. Zeuner, A. Tünnermann, S. Nolte, M. Segev, and A. Szameit, “Strain-induced pseudomagnetic field and photonic landau levels in dielectric structures,” *Nature Photonics* **7**, 153–158 (2012).
- ¹¹Y. Lumer, M. A. Bandres, M. Heinrich, L. J. Maczewsky, H. Herzig-Sheinfux, A. Szameit, and M. Segev, “Light guiding by artificial gauge fields,” *Nature Photonics* **13**, 339–345 (2019).
- ¹²K. Fang, Z. Yu, and S. Fan, “Realizing effective magnetic field for photons by controlling the phase of dynamic modulation,” *Nature Photonics* **6**, 782–787 (2012).
- ¹³N. Goldman and J. Dalibard, “Periodically driven quantum systems: Effective hamiltonians and engineered gauge fields,” *Physical Review X* **4** (2014), 10.1103/physrevx.4.031027.
- ¹⁴C. Jörg, F. Letscher, M. Fleischhauer, and G. von Freymann, “Dynamic defects in photonic floquet topological insulators,” *New Journal of Physics* **19**, 083003 (2017).
- ¹⁵E. Lustig, S. Weimann, Y. Plotnik, Y. Lumer, M. A. Bandres, A. Szameit, and M. Segev, “Photonic topological insulator in synthetic dimensions,” *Nature* **567**, 356–360 (2019).
- ¹⁶C. Jörg, G. Queralto, M. Kremer, G. Pelegrí, J. Schulz, A. Szameit, G. von Freymann, J. Mompert, and V. Ahufinger, “Artificial gauge field switching using orbital angular momentum modes in optical waveguides,” *Light: Science & Applications* **9** (2020), 10.1038/s41377-020-00385-6.
- ¹⁷Y. Aharonov and D. Bohm, “Significance of electromagnetic potentials in the quantum theory,” *Phys. Rev.* **115**, 485–491 (1959).
- ¹⁸H. Batelaan and A. Tonomura, “The aharonov–bohm effects: Variations on a subtle theme,” *Physics Today* **62**, 38–43 (2009).
- ¹⁹T. T. Wu and C. N. Yang, “Concept of nonintegrable phase factors and global formulation of gauge fields,” *Physical Review D* **12**, 3845–3857 (1975).
- ²⁰J. Vidal, R. Mosseri, and B. Douçot, “Aharonov–bohm cages in two-dimensional structures,” *Physical Review Letters* **81**, 5888–5891 (1998).
- ²¹D. Leykam, A. Andreanov, and S. Flach, “Artificial flat band systems: from lattice models to experiments,” *Advances in Physics: X* **3**, 1473052 (2018).
- ²²C. C. Abilio, P. Butaud, T. Fournier, B. Pannetier, J. Vidal, S. Tedesco, and B. Dalzotto, “Magnetic field induced localization in a two-dimensional superconducting wire network,” *Physical Review Letters* **83**, 5102–5105 (1999).
- ²³M. Rizzi, V. Cataudella, and R. Fazio, “Phase diagram of the bose-hubbard model with T3symmetry,” *Physical Review B* **73** (2006), 10.1103/physrevb.73.144511.
- ²⁴S. Mukherjee, M. D. Liberto, P. Öhberg, R. R. Thomson, and N. Goldman, “Experimental observation of aharonov–bohm cages in photonic lattices,” *Physical Review Letters* **121** (2018), 10.1103/physrevlett.121.075502.
- ²⁵M. Kremer, I. Petrides, E. Meyer, M. Heinrich, O. Zilberberg, and A. Szameit, “A square-root topological insulator with non-quantized indices realized with photonic aharonov–bohm cages,” *Nature Communications* **11** (2020), 10.1038/s41467-020-14692-4.
- ²⁶V. Brosco, L. Pillozzi, R. Fazio, and C. Conti, “Non-abelian thouless pumping in a photonic lattice,” (2020), arXiv:2010.15159 [cond-mat.mes-hall].
- ²⁷S. Longhi, “Aharonov–bohm photonic cages in waveguide and coupled resonator lattices by synthetic magnetic fields,” *Optics Letters* **39**, 5892 (2014).
- ²⁸D. N. Christodoulides, F. Lederer, and Y. Silberberg, “Discretizing light behaviour in linear and nonlinear waveguide lattices,” *Nature* **424**, 817–823 (2003).
- ²⁹R. A. Vicencio, C. Cantillano, L. Morales-Inostroza, B. Real, C. Mejía-Cortés, S. Weimann, A. Szameit, and M. I. Molina, “Observation of localized states in lieb photonic lattices,” *Physical Review Letters* **114**, 245503 (2015).
- ³⁰S. Xia, Y. Hu, D. Song, Y. Zong, L. Tang, and Z. Chen, “Demonstration of flat-band image transmission in optically induced lieb photonic lattices,” *Opt. Lett.* **41**, 1435–1438 (2016).
- ³¹B. Real, C. Cantillano, D. López-González, A. Szameit, M. Aono, M. Naruse, S.-J. Kim, K. Wang, and R. A. Vicencio, “Flat-band light dynamics in stub photonic lattices,” *Scientific Reports* **7** (2017), 10.1038/s41598-017-15441-2.
- ³²D. R. Hofstadter, “Energy levels and wave functions of bloch electrons in rational and irrational magnetic fields,” *Physical Review B* **14**, 2239–2249 (1976).
- ³³D. Langbein, “The tight-binding and the nearly-free-electron approach to lattice electrons in external magnetic fields,” *Physical Review* **180**, 633–648 (1969).
- ³⁴D. Hülge and B. Paredes, “Chiral ladders and the edges of quantum hall insulators,” *Physical Review A* **89**, 023619 (2014).
- ³⁵T. Ozawa, H. M. Price, A. Amo, N. Goldman, M. Hafezi, L. Lu, M. C. Rechtsman, D. Schuster, J. Simon, O. Zilberberg, and I. Carusotto, “Topological photonics,” *Rev. Mod. Phys.* **91**, 015006 (2019).
- ³⁶T. Ozawa and H. M. Price, “Topological quantum matter in synthetic dimensions,” *Nature Reviews Physics* **1**, 349–357 (2019).
- ³⁷E. Cohen, H. Larocque, F. Bouchard, F. Nejdassattari, Y. Gefen, and E. Karimi, “Geometric phase from aharonov–bohm to pancharatnam–berry and beyond,” *Nature Reviews Physics* **1**, 437–449 (2019).
- ³⁸K. Fang, Z. Yu, and S. Fan, “Photonic aharonov–bohm effect based on dynamic modulation,” *Physical Review Letters* **108** (2012), 10.1103/physrevlett.108.153901.
- ³⁹J. Vidal, B. Douçot, R. Mosseri, and P. Butaud, “Interaction induced delocalization for two particles in a periodic potential,” *Physical Review Letters* **85**, 3906–3909 (2000).
- ⁴⁰B. Douçot and J. Vidal, “Pairing of cooper pairs in a fully frustrated josephson-junction chain,” *Physical Review Letters* **88** (2002), 10.1103/physrevlett.88.227005.